24th INTERNATIONAL CONGRESS ON SOUND AND VIBRATION
23–27 July 2017, London

REAL-TIME PHYSICAL MODEL OF AN AEOLIAN HARP

Rod Selfridge, David J. Moffat, Joshua D. Reiss
Centre for Digital Music, EECS Dept., Queen Mary University of London, Mile End Road, UK.
email: r.selfridge@qmul.ac.uk

Eldad J. Avital
Centre for Simulation & Applied Mech., SEMS Dept., Queen Mary University of London, Mile End Road, UK.

A real-time physical sound synthesis model of an Aeolian harp is presented. The model uses semi-empirical fluid dynamics equations to inform its operation, providing suitable parameters for users to interact. A basic wind model is included as well as an interface allowing user adjustable parameters. Sounds generated by the model were subject to objective measurements against real-world recordings, which showed that many of the physical properties of the harp were replicated in our model, but a possible link between harmonics and vibration amplitude was not. A perceptual test was performed, where participants were asked to rate sounds in terms of how plausible they were in comparison with spectral modelling synthesis and recorded Aeolian Harp samples. Evaluation showed that our model performed as well as an alternative non-physical synthesis method, but was not as authentic as actual recorded samples.
Keywords: Sound Synthesis, Physical Model, Real-Time, Aeolian Harp.

1. Introduction

An Aeolian harp is a string instrument that makes a musically pleasing sound when wind passes over it. An example of an Aeolian harp is shown in Fig. 1. Fences, electrical wires, etc. can all be unintentional aeolian harps, if producing a harmonic sound when interacting with wind. The aim of this research was to create a sound synthesis model based on the physics of the Aeolian harp. The model operates in real-time, giving users a number of relevant parameters allowing them to model a wide range of harps. We used *semi-empirical* equations in which an assumption or generalisation has been made to simplify the calculation or yield results in accordance with observations.

An Aeolian tone is an aeroacoustic sound generated as air flows around an object. As air flows around a cylinder vortices are shed from opposite sides creating oscillating lift and drag forces. Full description of this process including a synthesis model is given in [1]. The sound of an Aeolian Harp is generated when the mechanical properties of the cylinder, (for a harp we refer to the cylinder as a string), interact with the aerodynamic forces that produce the Aeolian tone. It is know that a string has a fundamental vibrating frequency depending on its length, mass and tension [2] and harmonics at integer multiples. When the Aeolian tone frequency, caused by vortex shedding, is approximately the same as the fundamental string frequency, or a harmonic, the string vibrates, creating a stronger sound. An Aeolian harp has a number of strings; as the wind rises and falls different harmonics are excited depending on the properties of each strings.

2. Related work

The method of excitation is an important part of the synthesis model [3], for a string this is most commonly striking/plucking or friction. Numerous papers have been published on these topics, [4, 5] being examples of plucked and friction models respectively. The model presented here differs from the more common excitation methods by using the wind as an excitation method.

Figure 1: Aeolian harp at South Carolina, by Prof Henry Gurr[1], reproduced by kind permission.

In [6] an electro/acoustic instrument was created called the Magnetic Resonator Piano, in which the strings are excited by electromagnetic actuators. This has common ground with our synthesis model due to the strings not being plucked or struck but excited by electromagnetic waves.

Historically there have been stringed instruments that used air as an exciting force. An Aeolian Monochord was an instrument where air was blown by the mouth or bellows over a portion of a string like a bow and string lengths are adjusted by the fingers. An Anemocorde is a modified Aeolian harp with a keyboard and pedals; air was pushed over the strings by bellows [7].

Digital audio effects and synthesis techniques are used in Jean-Claude Risset musical piece *Avel*, a study of the wind [8]. Risset evokes Aeolian type sounds of the harp and flute, rising and falling to stylise the wind.

3. Physics behind the harp

3.1 Frequency Calculations

As air flows around a string, vortices are shed from alternate sides creating oscillating forces. These forces generate an Aeolian tone, the fundamental frequency of which is often called the Strouhal frequency f_s. The Strouhal number S_t is a variable that describes the relationship between the Strouhal frequency, air speed u, and diameter d shown in Eq. 1. The Strouhal number is ≈ 0.2 and can be calculated from the Reynolds number R_e, which is a measure of the flow unsteadiness as air flows past the string (see [1] for more details).

$$S_t = \frac{f_s\, d}{u} \tag{1}$$

The natural harmonic frequencies of a string f_η are calculated in Eq. 2 from tension T, length l and linear mass μ, where η is the harmonic number.

$$f_\eta = \frac{\eta}{2l}\sqrt{\frac{T}{\mu}} \tag{2}$$

When the Strouhal frequency approaches one of the natural harmonics of the string a phenomenon called *Vortex Induced Vibration* occurs in the string, [9]. One effect of this is that the frequency of vortex shedding f_v remains approximately constant over a range of airspeed, different from the calculated f_s. This is known as *lock-in*.

[1]Further details of Prof Gurr's work can be found at - http://web.usca.edu/math/faculty-sites/henry-gurr/aeolian.dot

3.2 Lock-In Calculations

To determine the range of airspeed where the string shedding frequency is locked-in, a dimensionless parameter called *reduced velocity* V is calculated. This is shown in Eq. 3, [10].

$$V = \frac{u}{2\pi d.f_\eta} \tag{3}$$

Figure 2a shows the relationship between the Strouhal, vortex shedding and natural vibrating frequencies. The minor discontinuity in Strouhal frequency is due to the piecewise linear manner in which it is calculated [1]. Plots given in [9–12] show vortex induced vibration around the fundamental natural frequency occurs between approximately $V = 0.8$ and $V = 1.27$. We chose both values as ideal lower and upper limits for illustration purposes, (blue line in Fig. 2a).

There is a hysteresis loop associated with the vibrations due to there being more than one vortex shedding mode present in the lock-in region [9–12], see Fig. 2b. The deviation of the vibrating string is given by the dimensionless parameter $A(t) = x(t)/d$, where $x(t)$ is the distance moved perpendicular to the flow. Calculating the maximum value for this, $A_{max}(t)$ starts with the fundamental string vibration equation given in [13] as:

$$\frac{\partial^2 x(t)}{\partial t^2} + \frac{b}{m}\frac{\partial x(t)}{\partial t} + \frac{k}{m}x(t) = 0 \tag{4}$$

where m, b, and k are the mass, damping and spring coefficients. From Eq. 4 we can represent the damping in terms of a proportional damping variable ζ, which is given as a percentage of critical damping [13] and shown in Eq. 5.

$$\frac{b}{m} = 4\zeta\pi f_\eta \tag{5}$$

Peak amplitude of the vibrating string is related to the damping through a combined mass-damping parameter α, [11]:

$$\alpha = m^* \zeta \tag{6}$$

where $m^* = \rho_m/\rho_f$, (ρ_m and ρ_f are the mass density of the string and air respectively). From [11] the relationship between the mass-damping parameter and maximum vibration amplitude $A_{max}(t)$ is dependent on the Reynolds number. For high R_e:

$$A_{max}(t) = [1 - 1.12\alpha + 0.30\alpha^2]\log_{10}(0.41R_e^{0.36}(t))$$

and for low R_e:

$$A_{max}(t) = 0.63[1 - 1.29\alpha + 0.59\alpha^2] \tag{7}$$

3.3 Frequency Spectrum

The sound produced while the string is vibrating in the lock-in region has a distinct frequency spectrum. In [14] it is found that the acoustic output of a string vibrating in the lock-in region has a central peak at the vortex shedding frequency f_v with harmonics at $f_{\eta\pm1}$, $f_{\eta\pm2}$, etc. (During lock-in $f_v \approx f_\eta$). Sideband amplitude decreases with distance from $f_v(t)$ similar to that of a Frequency Modulated (FM) signal, with the carrier frequency equivalent to f_v, modulated by a difference frequency f_d:

$$f_d = f_{\eta+1} - f_v \tag{8}$$

A low frequency signal at f_d is also present, [14], with sidebands at $2f_d$, $3f_d$, etc. again with decreasing amplitude as the sideband number increases. Out with the lock-in region the vortex shedding frequency $f_v \approx f_s$ as shown in Fig. 2a; f_v varies directly with u, (as does f_d).

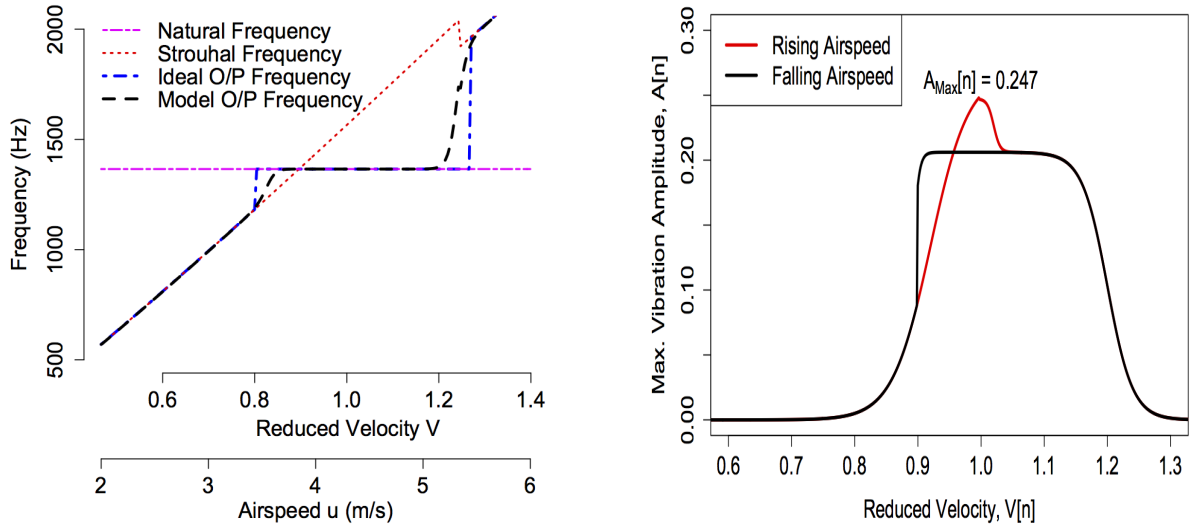

(a) (b)

Figure 2: (a) Ideal lock-in conditions and model output at 6th harmonic (1365.4Hz). Lock-in at 5th and 7th harmonics removed for clarity. $d = 0.0005m$, $l = 0.61m$, $\rho_m = 2432.2kg/m^3$, $T = 36.81N$, $\zeta = 0.006$ and $\eta = 1$. (b) Implementation of hysteresis curve showing maximum vibration amplitude in the lock-in region. $\zeta = 0.002$, $d = 6.1\text{x}10^{-4}$m, $l = 0.65$m, $\rho_m = 6649$kg/m^2, $T = 70.78$N.

4. Implementation

Our model was realised in Pure Data, a real-time graphical data flow programming language.

4.1 Discrete Frequency Calculations

The Aeolian tone model from [1] calculates the Strouhal frequency $f_s[n]$ value. The fundamental string vibration frequency f_1 is calculated from Eq. 2 setting $\eta = 1$. The nearest harmonic mode $\eta[n]$ is calculated by Eq. 9.

$$\eta[n] = \text{round}\left(\frac{f_s[n]}{f_1}\right) \tag{9}$$

Therefore the nearest string harmonic is:

$$f_\eta[n] = \eta[n] f_1 \tag{10}$$

4.2 Vibration Magnitude Calculations

The reduced velocity $V[n]$ is calculated from a discrete implementation of Eq. 3. Sigmoid functions, chosen to have characteristics similar to plots given in [9–12], are used to calculate the normalised vibration amplitude $A[n]$ for the given value of $V[n]$ (hysteresis property is included). Calculating the mass-damping parameter $\alpha[n]$ it was assumed that the relationship of b/m, given in Eq. 5, remains constant for all harmonic modes giving:

$$4\zeta\pi f_\eta[n] = 4\eta[n]\zeta\pi f_1 \tag{11}$$

which increases the damping factor as harmonic mode number increases. Applied to Eq. 6, this gives:

$$\alpha[n] = m^*\, \eta[n]\zeta \tag{12}$$

The value for the maximum vibration amplitude $A_{max}[n]$ is calculated using Eq 7. A value of $R_e[n] = 500$ is the transition value between the two conditions [11] . $A[n]$ is scaled by $A_{max}[n]$ giving the actual vibration magnitude. Fig. 2b shows a typical response from our implementation.

4.3 Modulation

The difference frequency $f_d[n]$ is obtained from a discrete implementation of Eq. 8. For a FM output [14], the carrier frequency is the vortex shedding frequency $f_v[n]$ giving:

$$y_{FM}[n] = \cos(2\pi(f_v[n] + \chi\cos(2\pi f_d[n]))) \tag{13}$$

where χ is the modulation index given as an user input. The low frequency modulated signal is calculated as:

$$y_{LFFM}[n] = 0.1\cos(2\pi(f_d[n] + \chi\cos(2\pi f_d[n]))) \tag{14}$$

where the multiplication factor of 0.1 corresponds to a similar reduction in power shown in [14].

4.4 Output Signal

When the string is out of lock-in the output is simply the Aeolian tone signal $g[n]$ as given in [1], ($f_v[n] = f_s[n]$). When the string is within lock-in $A_{max}[n]$ is dependant on $V[n]$ and α, ($f_v[n] = f_\eta[n]$). The acoustic intensity of the Aeolian tone greatly increases during lock-in partially due to the increase in vortex correlation along the length of the string, [12, 15]. This is approximated in our model by adding $200A_{max}[n]$ to the value calculated in [1]. The vibration amplitude $A_{max}[n]$ is applied as a gain, giving a discrete signal $y[n]$ as:

$$y[n] = g[n] + \Lambda\, A_{max}[n]\big(y_{FM}[n] + y_{LFFM}[n]\big) \tag{15}$$

where Λ is a scaling factor between the Aeolian tone and FM output. In this instance Λ was set to $5\text{x}10^{-5}$ which provided an acceptable balance between the two outputs. Note, $A_{max}[n] \to 0$ when out of lock-in or at high harmonic numbers.

An adapted wind model from [16] allows user control of the windspeed and amount of underlying gusts. The PureData patch created using this implementation is available for download, (along with sounds used for subjective evaluation).[2]

5. Results and Analysis

The Aeolian harp recording used for the objective test as well as the majority of the subjective tests were from Roger Winfield's CD Windsongs [17]. Details of the harps used are limited but they have been described as 6 foot taller or more [18]: the tension, diameter and string density are all unknown. Professor Gurr states on his website[1] that the recordings are of very good quality, paraphrasing Roger Winfield that the sounds were edited from recordings taken over a number of months. Prof. Gurr is also of the opinion that the recordings may have been slowed down in order to reach some of the pitches heard. Some of the other sounds used in the listening tests, real and SMS, were taken from YouTube clips of Aeolian harps and provenance cannot be confirmed.

5.1 Objective Evaluation

The value of an objective evaluation, comparing our model output with a recording from the Windsongs CD [17], is that we can identify the similarities and differences in signal properties, highlighting where our model performs well against real harps as well as where it may fail to capture some characteristics. It is conceded that the best test would be with audio from a real harp in which physical properties are known but even with harp details we would wish to have wind speed data corresponding to the audio recording enabling us to perform an exact comparison.

Spectrograms and time waveforms of a recorded Aeolian harp and one from our synthesised physical model are shown in Fig. 3. It should be noted that, as well as physical properties, the recording method for the real Aeolian harp is unknown.

[2] https://code.soundsoftware.ac.uk/projects/aeolianharp

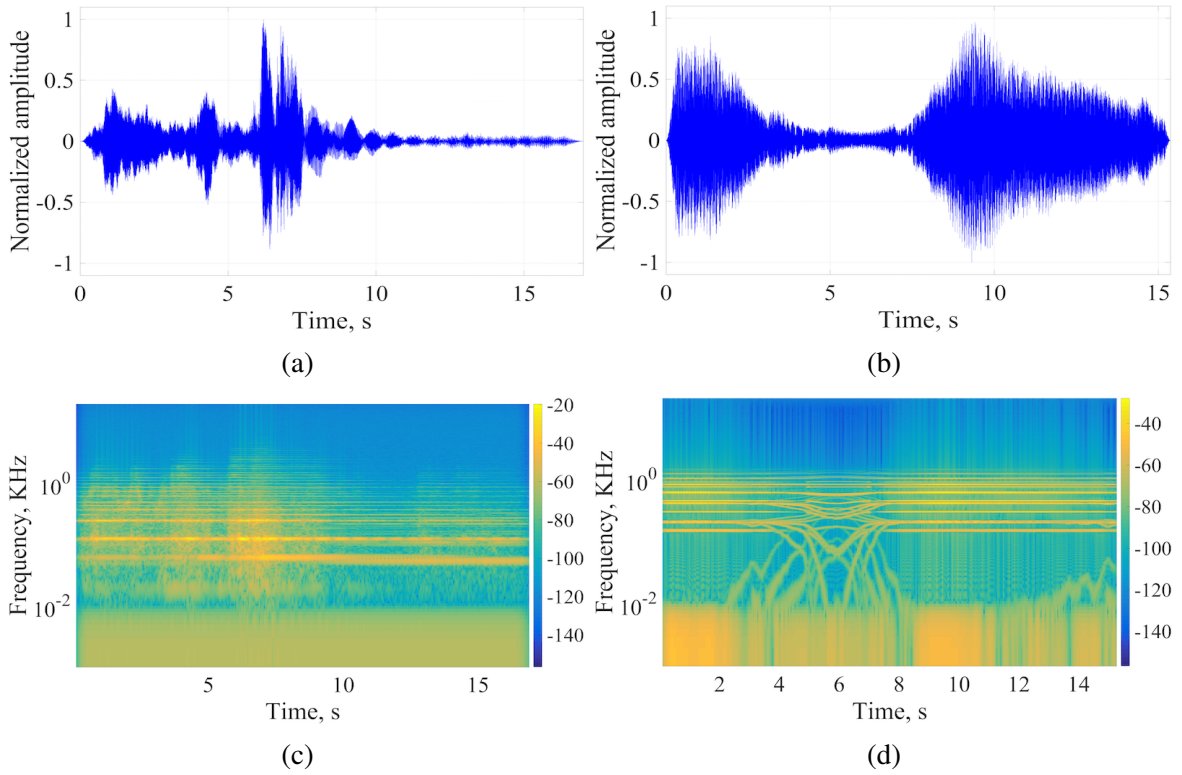

Figure 3: Time plots and spectrograms of an Aeolian harp - recorded ((a) & (c)) and physical model ((b) & (d)) Aeolian harp.

One of the main differences visible between the two spectrograms are the number of harmonics in the recorded version. Possible reasons for the disparity are: the frequency modulation of the sound from the real harp creates more sidebands than the synthesis model, the physical harp that this recording was obtained has more strings than the synthesis model which are tuned to produce higher frequencies, or there is a fluid dynamics / mechanics interaction that is not understood and not captured by the synthesis model. The synthesis model goes some way to mitigate the first two points by allowing the user to vary the modulation index, expanding and compressing the number of frequency sidebands. Further, the model has up to 13 strings available to the user which can be tuned to individual frequencies, each with their own harmonics.

In Fig. 3c the number of harmonics are not constant. The areas with a higher number of partials corresponds to areas of higher amplitude in the the time waveforms, Fig. 3a. This could indicate an additional fluid dynamics / mechanical interaction as stated above. Any such link is not replicated by our model, as seen in Fig. 3d.

In both spectrograms there are a series of fixed harmonic frequency components, steady for a period of time. This is due to the frequencies being held constant in the lock-in region, so despite constant fluctuations in the wind and hence airspeed, similar small scale fluctuations are not visible in either spectrogram. Conversely, the strength of partials changing and evolving is visible in both plots. This is due to the variation in the value of A as shown in Fig. 2a and clearly visible as magnitude variations in both time waveforms, Figs. 3a and 3b.

The greatest level of amplitude variation is witnessed in the waveform given in Fig. 3b. In this example the amount of variation in windspeed (gusts), is low. There are 4 strings used in the model with the vortex shedding frequency approximately 615Hz. As the gusts are quite small in their variation it is easier to see the amplitude changes; as the windspeed $u[n]$, varies the reduced velocity $V[n]$, varies changing the value of $A_{max}[n]$ and hence the gain.

The varying frequency seen starting after ≈ 3 seconds in Fig. 3d is where the strings are coming out of lock-in, returning to $f_v = f_s$ where shedding varies with windspeed. The low frequency f_d can also be seen varying as would be expected from Eq. 8. It may be that the amplitude of the Aeolian tone out with lock-in has been made larger in our model than the actual recorded harp and why it is

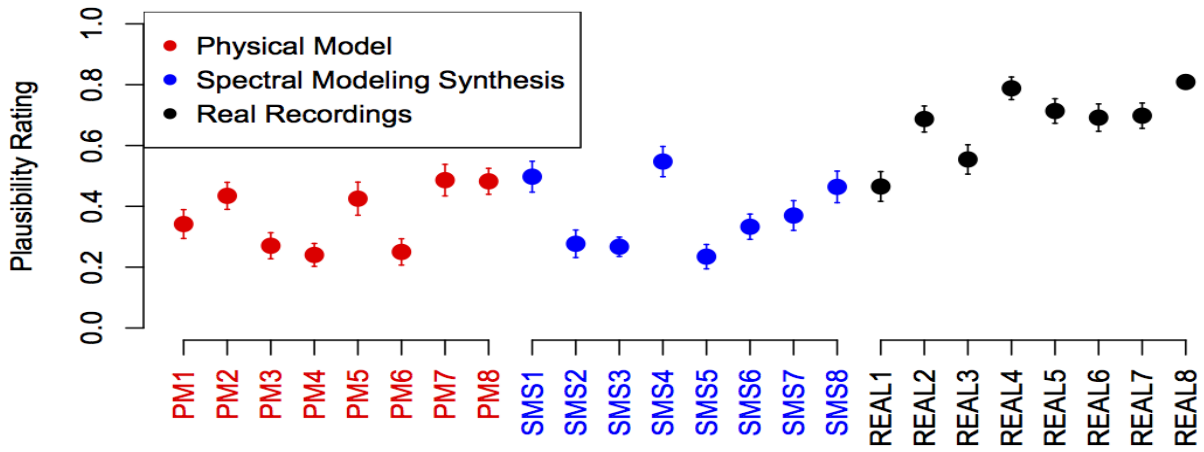

Figure 4: Mean values, including standard error bars for each clip.

not seen in Fig. 3c, or the recorded harp does not fully come out of lock-in within the time frame we are examining and hence no variation is seen.

5.2 Subjective Evaluation

To evaluate how close our model sounds like an Aeolian harp, a perceptual test was undertaken. Since Aeolian harps are not common, participants were given training to assist identification of an Aeolian harp. Prior to the start participants were invited to watch a short video explaining the Aeolian harp and how it sounds[3]. Thereafter participants were asked to rate four groups of Aeolian harp sounds, each having six sound clips, two from the physical model, two created by spectral modelling synthesis (SMS) [19], and two recordings of actual harps giving 24 clips overall. The SMS clips are produced by analysis of real recordings (not used in the test) and then synthesised from these, therefore wind generation should not be an issue with these. There were 32 participants in the tests, 22 male and 10 female, aged from 16 years old to 77 years old with an average age of 36. Eight participants had previously heard an Aeolian harp. The Web Audio Evaluation Tool [20] was used to capture the participants preferences.

The mean perceptual rating for all 24 clips is shown in Fig. 4. It can be seen that the real recordings receives the highest plausibility rating; there is little between the two synthesis methods, both averaging 0.37 overall. One factor that might reduce the perceptual rating of the physical model sounds is that the scalar value generated to represent the airspeed is from a wind synthesis model taken from [16]. It might be the case that there are subtleties that are not captured by this wind synthesis model that drives the real harps.

It should also be noted that the recording of real Aeolian harps were stereo while the ones generated from the synthesis model were mono. This may have had an influence on the plausibility rating as a stereo audio clip may be perceived as more realistic.

6. Conclusions

The real-time physical model of an Aeolian harp has been presented. Fundamental equations from fluid dynamics have been used to calculate the relevant equations as well as the mechanical properties of the strings. Objective evaluation of the model has been carried out which revealed our model captures a number of the fundamental characteristics of the Aeolian harp. There appears to be an increased number of harmonics in the recorded sounds which vary as the sounds evolve and windspeed changes. This property has not been captured by our model and further study may reveal a link between the vibration amplitude and modulation index.

An advantage of our model over other synthesis methods is the parameterisation of the model that is based on physical properties of the strings and therefore able to replicate real world harps. Sounds

[3] https://www.youtube.com/watch?v=d6c6-u3MQDk

produced from our synthesis model will differ from those from physical Aeolian harps in that physical models either require electronic pick-ups, like guitar pick-ups, or are coupled to a soundboard in order to amplify the sounds. We do not simulate these processes and hence our sounds will not include any associate artefacts. Likewise, we do not simulate any coupling or fluid dynamic interactions if two strings are close together.

Acknowledgments

Thanks to Prof Henry Gurr, University of South Carolina for his encouragement and suggestions. Supported by EPSRC grant EP/G03723X/1.

References

1. Selfridge, R., et al. Physically derived synthesis model of Aeolian tones (Winner of Best Student Paper Award), *141st Audio Engineering Society Convention USA*, (2016).
2. Fletcher, N. H. and Rossing, T., *The physics of musical instruments*, Springer Science and Business Media (2012).
3. Cook, P. R., *Real sound synthesis for interactive applications*, CRC Press (2002).
4. Valimaki, V., et al. Plucked-string synthesis algorithms with tension modulation nonlinearity, *IEEE Int. Conf. Acoustics, Speech, and Signal Processing*, (1999).
5. Serafin, S., et al. Friction and application to real-time physical modeling of a violin, *Proc. of the International Computer Music Conference*, (1999).
6. McPherson, A. The magnetic resonator piano: Electronic augmentation of an acoustic grand piano, *J. New Music Research*, (2010).
7. Engel, C. Aeolian music, *The Musical Times*, (1882).
8. Risset, J. C. Examples of the musical use of digital audio effects, *J. New Music Research*, (2002).
9. Sarpkaya, T. A critical review of the intrinsic nature of vortex-induced vibrations, *J. Fluids and Structures*, (2004).
10. Brika, D. and Laneville, A. Vortex-induced vibrations of a long flexible circular cylinder, *J. Fluid Mechanics*, (1993).
11. Govardhan, R. and Williamson, C. Defining the 'modified Griffin plot' in vortex-induced vibration: revealing the effect of reynolds number using controlled damping, *J. Fluid Mechanics*, (2006).
12. Gabbai, R. and Benaroya, H. An overview of modeling and experiments of vortex-induced vibration of circular cylinders, *J. Sound and Vibration*, (2005).
13. Takács, G. and Rohal'-Ilkiv, B., *Model Predictive Vibration Control: Efficient Constrained MPC Vibration Control for Lightly Damped Mechanical Structures*, Springer Science & Business Media (2012).
14. Van Atta, C. and Gharib, M. Ordered and chaotic vortex streets behind circular cylinders at low reynolds numbers, *J. Fluid Mechanics*, (1987).
15. Bearman, P. W. Vortex shedding from oscillating bluff bodies, *Annual Review of Fluid Mechanics*, (1984).
16. Farnell, A., *Designing sound*, MIT Press Cambridge (2010).
17. Winfield, R., (1993), *Windsongs*. Saydisc Records.
18. DeBlieu, J., *Wind: How the flow of air has shaped life, myth, and the land*, Counterpoint Press (2006).
19. Zölzer, U., et al., *DAFX: Digital Audio Effects*, Wiley Online Library (2002).
20. Jillings, N., et al. Web audio evaluation tool: A browser-based listening test environment, *Sound and Music Computing*, (2015).